Integral Equation Modeling of Doubly Periodic Structures With an Efficient PMCHWT Formulation

Samuel Nosal, Paul Soudais, Jean-Jacques Greffet

Integral Equation Modeling of Doubly Periodic Structures With an Efficient PMCHWT Formulation

Samuel Nosal, Paul Soudais, and Jean-Jacques Greffet

***Abstract*—A surface integral equation modeling is described for complex doubly periodic structures. To avoid long computations of the slowly convergent pseudoperiodic Green's function, fictitious surfaces between translated unit cells are set in order to bound regions of the structure within the symmetry cell and use the free-space Green's function. The integral operators on top and bottom surfaces are computed with an algorithm originally used for planar frequency-selective surfaces. This approach uses a unique periodic PMCHWT formulation in all the regions, with two different kinds of Green's function. The method and its advantages are illustrated by two cases in the near-IR domain and in the radar domain. A frequency selective structure is studied, that shows a large flat-top bandwidth under oblique incidence and TM polarization.**

***Index Terms*—Boundary integral equations (BIE), frequency selective surfaces (FSS), hybrid method, metamaterials, method of moments (MoM), periodic Green's function.**

I. Introduction

DOUBLY-PERIODIC (or biperiodic) structures can be used to design frequency selective radomes or antenna substrates. At IR or optical wavelengths, they can be used as antireflective coatings or filters. These structures are examples of metamaterials and photonic crystals. As devices built on these structures are getting more and more complex, there is a need for versatile numerical methods for the scattering from complex biperiodic structures with short computation times.

Purposefully, we present here a method based on surface integral equations (SIE), which is able to handle biperiodic structures with a finite thickness made up of an arbitrary configuration of perfectly conducting (PEC) and homogeneous isotropic dielectric regions.

Numerical methods have been developed for decades to model the diffraction by periodic structures, but they strike a compromise between applications to specific geometries (e.g. layered planar structures), accuracy and computation time.

Among them, the SIE-based methods take a large place: the method of moments for planar FSS [1]–[3] has been proven a fast and accurate method. It is limited to FSS made of infinitely thin metallic or resistive patches, whose shapes can be described on a regular grid. Two extensions for stacked FSS separated by dielectric layers can be used. The scattering problem can be handled by a S-matrix cascading technique [1] or layered Green's functions [4].

If the symmetry cell is made of regions of 3D arbitrary shape, one can use volume methods with periodic boundary conditions (PBC) based on finite difference time domain (FDTD) method [5] or finite element (FE) methods (e.g. [6] and [7]). But the number of unknowns for volume formulations will usually be much higher than for surface formulations.

Another group of methods is based on pseudoperiodic SIE. They involve the pseudoperiodic Green's function, which is a very slowly convergent double series. Several techniques to accelerate the convergence of this series have been studied, some of them have been recently compared in [8].

A pseudoperiodic SIE method was proposed in [9]. A pseudoperiodic PMCHWT (from Poggio, Miller, Chang, Harrington, Wu and Tsai) formulation was used in all the regions. The large computational cost of the Green's function for doubly periodic problems was alleviated by a tabulation of both the pseudoperiodic Green's function and its gradient.

In order to reduce the number of evaluations of the pseudoperiodic Green's function, hybrid methods were suggested: by "hybrid method", we designate a method that solves differently the outer region (often vacuum) and the inner region (the doubly periodic structure). In [10], the outer infinite regions are treated with SIE using the pseudoperiodic Green's function, while the inner bounded regions in the biperiodic structure are treated with a FE method. These methods are often referred to as hybrid finite element-boundary integral (FE-BI) methods. Their main problem is that the (volume) FE method requires the creation of many degrees of freedom.

A hybrid method using two different SIE formulations was developed in [11]. The internal regions of the structure were bounded with fictitious surfaces, and then the free-space Green's function was used inside the structure. This resulted in a tremendous reduction in the assembly time, usually offsetting by far the extra-solution time due to the extra-unknowns on the fictitious surfaces. The outside problem was formulated with a MoM derived from the MoM for planar FSS of [1]–[3].

In this paper, we present a hybrid method that uses only one integral formulation, but both the pseudoperiodic Green's func-

S. Nosal was with EM2C Laboratory, École Centrale Paris. He is now with the Laboratory for Electromagnetic Fields and Microwave Electronics, Swiss Federal Institute of Technology, ETH-Zentrum, ETZ K97, CH-8092 Zurich, Switzerland (e-mail: samuel.nosal@ensta.org).

P. Soudais is with Dassault-Aviation, 92210 Saint-Cloud, France (e-mail: paul.soudais@dassault-aviation.com).

J.-J. Greffet was with EM2C Laboratory, École Centrale Paris. He is now with the Charles-Fabry Laboratory, Institut d'Optique, Université Paris Sud, CNRS, F-91127 Palaiseau cedex, France (e-mail: jean-jacques.greffet@institutoptique.fr).

tion and the free-space Green's function by using fictitious surfaces to bound the inner regions of a unit cell.

The key point of the method, as presented in Section II, is the use of an adapted PMCHWT formulation [12], which is often used for general purpose codes dealing with several dielectric or conducting regions and impedance conditions: for 2D and 3D scatterers [13], for bodies of revolution [14], for large scatterers [15]. This formulation requires the computation of contributions from the entire boundary of regions neighboring the symmetry cell and we will show how to recover these terms in an easy way. To the best of our knowledge, it is the first time that a pseudoperiodic formulation is presented, that uses a unique PMCHWT formulation for all the regions, including regions bounded by fictitious surfaces with PBC.

Another important point is that the PMCHWT contribution from the top and bottom unbounded regions are efficiently computed thanks to a method derived from a Method of Moments (MoM) specific to planar frequency selective surfaces (FSS). This is achieved by using triangular RWG functions on part of the mesh and rooftop basis functions on top and bottom surfaces, as presented in Section III. Note that in [11], the top planar surface was meshed with isosceles rectangle triangles and a linear combination of the triangular basis functions had to be made to obtain rooftop basis functions on the top surface.

The use of these techniques makes it possible to obtain a numerical method, whose computational time is similar to that of a case where the symmetry cell would be computed as an isolated object (i.e. a non-periodic 3D case with similar number of unknowns), as illustrated by the validation cases in Section IV.

II. Pseudoperiodic PMCHWT Formulation

A. Description of the Pseudoperiodic Problem

1) Biperiodic Scattering Structure: A biperiodic diffractive structure consists of a unit cell which is repeated over two directions of periodicity, given by the vectors $\mathbf{T}_1 = T_1\hat{x}$ and $\mathbf{T}_2 = T_2\hat{y}$, as schematized on Fig. 1. Note than in this work, $\mathbf{T}_1$ and $\mathbf{T}_2$ could be made non orthogonal without any modification except in Section III-B. where the algorithm for planar FSS should be used in its skewed lattice version [1]. The unit cell is composed of an arbitrary number of homogeneous material regions with complex permittivity ε and permittivity μ or PEC regions. The array is of finite thickness and is placed between two semi-infinite regions, generally air or PEC.

2) Scattering Problem: An incident plane wave $(\mathbf{E}^{inc}, \mathbf{H}^{inc})$ impinges on the biperiodic scattering structure. The time-harmonic dependence is taken as $e^{+j\omega t}$. At a given frequency, the incident field is completely defined by the components of its normalized wave vector along the x and y axes (k_x/k^{inc} and k_y/k^{inc}, from which k_z/k^{inc} is deduced), its polarization (TE or TM), the region where its source is located (top or bottom) and its amplitude, where $k^{inc} = \omega/c$, c being the speed of light in the region where the source is located.

Due to the pseudoperiodicity of the incident field, the biperiodicity of the scattering structure and the linearity of Maxwell's equations, the scattered field is pseudoperiodic: it is only necessary to find its values on the symmetry cell. The values of the field in any other cell can be calculated using the following relation

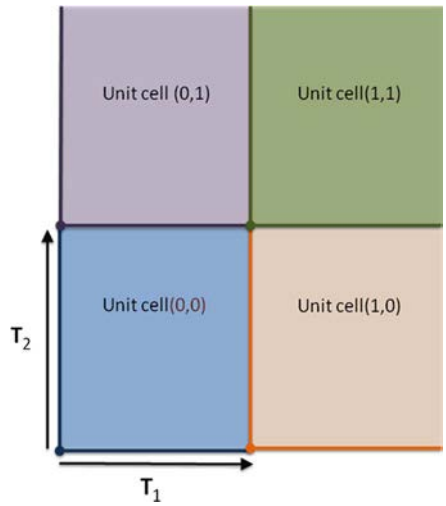

Fig. 1. Definition of the reference unit cell, which is repeated according to the translation vectors $\mathbf{T}_1$ and $\mathbf{T}_2$. Note that only the left and bottom boundaries with the translated cells belong to the reference unit cell (0,0).

$$\mathbf{E}^S(\mathbf{r} + n\mathbf{T}_1 + m\mathbf{T}_2) = \mathbf{E}^S(\mathbf{r}) \exp\left(-j\varphi(n,m)\right) \quad (1)$$

where $\varphi(n,m) = n\mathbf{k}^i\cdot\mathbf{T}_1 + m\mathbf{k}^i\cdot\mathbf{T}_2$ is the phase coefficient, $\mathbf{k}^i$ being the incident wave vector. Pseudoperiodic boundary conditions on opposite faces of the symmetry cell are a consequence of (1).

B. PMCHWT Formulation for 3D Problems

1) Electric and Magnetic Field Integral equations (EFIE and MFIE): For the sake of simplicity, we give here the outline of the formulation in the case where there are only two homogeneous dielectric regions, separated by a closed surface S. The extension to an arbitrary number of regions can be easily achieved. Following J.-M. Jin's notation [14], we can write in each region d both the electric field integral equation (EFIE)

$$-\frac{1}{2}\mathbf{M}_d + j\hat{n}_d \times \overline{K}(\mathbf{M}_d) + Z_d\hat{n}_d \times L_d(\mathbf{J}_d) = \hat{n}_d \times \mathbf{E}^{inc} \text{on } S \quad (2)$$

and the magnetic field integral equation (MFIE)

$$\frac{j}{2}\mathbf{J}_d + \hat{n}_d \times \overline{K}_d(\mathbf{J}_d) + \frac{j}{Z_d}\hat{n}_d \times L_d(\mathbf{M}_d) = jZ_d\hat{n}_d \times \mathbf{H}^{inc} \text{on } S \quad (3)$$

where $\mathbf{M}_d = \mathbf{E} \times \hat{n}_d$, $\mathbf{J}_d = Z_0\hat{n}_d \times \mathrm{H}$,

$$L_d(\mathbf{X}) = jk_d \iint_S \left[\mathbf{X}(\mathbf{r}')G_d(\mathbf{r},\mathbf{r}') + \frac{1}{k_d^2}\nabla'\cdot\mathbf{X}(\mathbf{r}')\nabla G_d(\mathbf{r},\mathbf{r}')\right] ds', \quad (4)$$

$$\overline{K}_d(\mathbf{X}) = -j \iint_{S-\{\mathbf{r}\}} \mathbf{X}(\mathbf{r}') \times \nabla' G_d(\mathbf{r},\mathbf{r}') ds' \quad (5)$$

and $Z_d = \sqrt{\mu_{r,d}/\varepsilon_{r,d}}$ being the relative impedance of the dielectric region d.

In these equations, $G_d(\mathbf{r},\mathbf{r}')$ is the free-space Green's function in the region d (=1 or 2) and the incident fields $\mathbf{E}^{inc}, \mathbf{H}^{inc}$ only exist in the region where their source is located. They are uniformly zero in the other region.

2) PMCHWT Formulation: The PMCHWT formulation is used for the scattering by composite dielectric objects. On the boundary S separating two dielectric regions (e.g. $\mathbb{R}^1$ and $\mathbb{R}^2$), the EFIE (2) and MFIE (3) from each region are summed to give the PMCHWT, using the fact that tangential fields are continuous across S: $\mathbf{J}_1 = -\mathbf{J}_2 = \mathbf{J}$ and $\mathbf{M}_1 = -\mathbf{M}_2 = \mathbf{M}$. Hence, the equations that are to be solved are

$$\begin{aligned}
&-\hat{n}_1 \times (\hat{n}_1 \times (Z_1 L_1(\mathbf{J}) + Z_2 L_2(\mathbf{J})))\\
&-\hat{n}_1 \times \left(j\hat{n}_1 \times \left(\overline{K}_1(\mathbf{M}) + \overline{K}_2(\mathbf{M})\right)\right)\\
&\quad = -\hat{n}_1 \times (\hat{n}_1 \times \mathbf{E}^{inc}), \qquad (6)\\
&-\hat{n}_1 \times \left(j\hat{n}_1 \times \left(\frac{1}{Z_1} L_1(\mathbf{M}) + \frac{1}{Z_2} L_2(\mathbf{M})\right)\right)\\
&-\hat{n}_1 \times \left(\hat{n}_1 \times \left(\overline{K}_1(\mathbf{J}) + \overline{K}_2(\mathbf{J})\right)\right)\\
&\quad = -\hat{n}_1 \times (jZ_0\hat{n}_1 \times \mathbf{H}^{inc}). \qquad (7)
\end{aligned}$$

The associated variational formulation of (6) and (7) is discretized by a boundary element method, with RWG and rooftop basis and test functions, both denoted by ψ (Galerkin method). Equation (6) is tested with ψ_J test functions and (7) is tested with ψ_M test functions.

The discretized operators read (e.g. [13]):

$$\begin{aligned}
\mathbf{L}_d(p,q) &= \left\langle L_d\left(\psi'_q\right), \psi_p \right\rangle_s\\
&= j \iint_{S\times S} \left\{ k_d G_d(\mathbf{r},\mathbf{r}') \left(\psi_p \cdot \psi'_q\right) \right.\\
&\qquad \left. - \frac{1}{k_d} G_d(\mathbf{r},\mathbf{r}') \left((\nabla_S \cdot \psi_p)\left(\nabla'_S \cdot \psi'_q\right)\right) \right\} ds ds'\\
&\quad d = 1,2 \qquad (8)\\
\overline{\mathbf{K}}_d(p,d) &= \left\langle K_d\left(\psi'_q\right), \psi_p \right\rangle_S\\
&= -j \iint_{S\times(S-\{\mathbf{r}\})} (\nabla' G_d(\mathbf{r},\mathbf{r}')) \cdot \left(\psi_p \times \psi'_q\right) ds ds'\\
&\quad d = 1,2. \qquad (9)
\end{aligned}$$

This leads to the following linear system, which can usually be solved directly:

$$\begin{pmatrix} Z_1\mathbf{L}_1 + Z_2\mathbf{L}_2 & \overline{\mathbf{K}}_1 + \overline{\mathbf{K}}_2 \\ \overline{\mathbf{K}}_1 + \overline{\mathbf{K}}_2 & \frac{1}{Z_1}\mathbf{L}_1 + \frac{1}{Z_2}\mathbf{L}_2 \end{pmatrix} \begin{pmatrix} J \\ jM \end{pmatrix} = \begin{pmatrix} E^{inc} \\ jZ_0 H^{inc} \end{pmatrix}. \qquad (10)$$

Note that we use $j\mathbf{M}$ unknowns instead of $\mathbf{M}$ unknowns in order to obtain a symmetrical discretized matrix [16].

This formulation can be generalized to an arbitrary number of dielectric regions. Due to the continuity of tangent fields, for an edge belonging to two or more dielectric regions numbered $\mathrm{d} = 1$ to k, there is one composite ψ_J basis and test function for J and one composite ψ_M basis and test function for M [17]. The value for a composite function ψ in region d is ψ^d (cf. Fig. 2). Note that it is necessary to use composite functions on every edge: on edges belonging to two dielectric regions, the composite function is made of two RWGs or two rooftops functions with opposite signs.

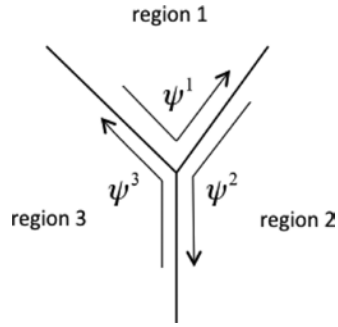

Fig. 2. Top view of a junction between several dielectric regions and composite function on a junction edge.

The PMCHWT formulation writes for ψ_J [13], [17]:

$$\begin{aligned}
\sum_{d=1,k} \left\{ \sum_{\psi'^d_J \in S^d} \left\langle Z_d \mathbf{L}_d\left(\psi'^d_J\right), \psi^d_J \right\rangle + j \sum_{\psi'^d_M \in S^d} \left\langle \overline{\mathbf{K}}_d\left(\psi'^d_M\right), \psi^d_J \right\rangle \right\}\\
= \sum_{d=1,k} \left\langle E^{inc,d}, \psi^d_J \right\rangle. \qquad (11)
\end{aligned}$$

The PMCHWT formulation writes for ψ_M [13], [17]:

$$\begin{aligned}
\sum_{d=1,k} \left\{ \sum_{\psi'^d_M \in S^d} \left\langle \frac{j}{Z_d} \mathbf{L}_d\left(\psi'^d_M\right), \psi^d_M \right\rangle + \sum_{\psi'^d_J \in S^d} \left\langle \overline{\mathbf{K}}_d\left(\psi'^d_J\right), \psi^d_M \right\rangle \right\}\\
= jZ_0 \sum_{d=1,k} \left\langle H^{inc,d}, \psi^d_M \right\rangle. \qquad (12)
\end{aligned}$$

Please recall that the incident field $(\mathbf{E}^{inc,d}, \mathbf{H}^{inc,d})$ is non-zero only in the region where the source is located. On PEC boundaries, $\mathbf{M} = 0$, and there are no test functions ψ_M and we write only (11) for test functions ψ_J. Note that (11) only includes contributions from dielectric regions.

C. Hybrid SIE Formulation: Fictitious Surfaces

A way to adapt the PMCHWT formulation to doubly periodic scatterers is to replace, in each unbounded region, the Green's function by the pseudoperiodic Green's function, i.e. the Green's function for a double array of point sources in this region. Each of these Green's functions satisfies the PBC (1).

We investigate here another way, following [11], to address the computational time issue: reducing as much as possible the number of evaluations of the pseudoperiodic Green's function. We add fictitious surfaces between the reference unit cell and its translated neighboring cells, as shown on Fig. 3. Thus the inner regions of the periodic structure are bounded, allowing the use of the free-space Green's function, whose computation cost is negligible.

D. Writing a Pseudoperiodic PMCHWT Formulation With Fictitious Surfaces

For the sake of simplicity, we first consider the case where two homogeneous regions bounded by fictitious surfaces fill the

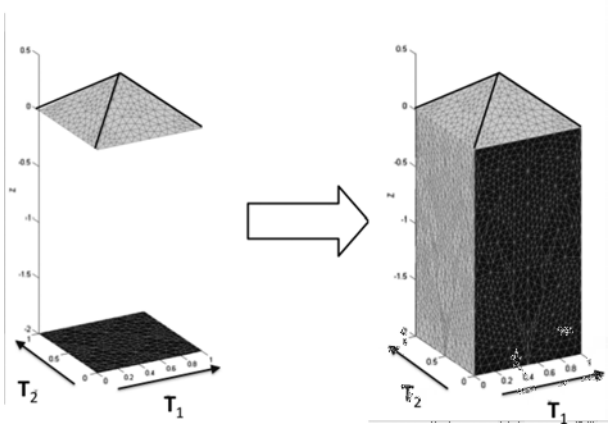

Fig. 3. Example of a pyramid array on a silicon slab. **Left**: mesh used for a 3D pseudoperiodic SIE. There are three infinite regions: the two outer regions are filled with air; the inner region is filled with silicon. **Right**: mesh used for the proposed hybrid method. Here only the outer regions are infinite and the inner region is bounded by adding four vertical fictitious surfaces.

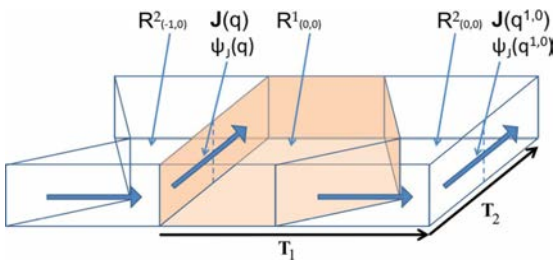

Fig. 4. Pseudoperiodic electric equivalent currents on two opposite fictitious surfaces with pseudoperiodic boundary conditions.

symmetry cell (Fig. 4). The mesh is assumed to have been created so that the surface meshes on opposite fictitious surfaces are identical. Only unknowns belonging to the (0,0) symmetry cell are considered. The values of the currents in other cells can be computed thanks to the PBC (1).

The pseudoperiodicity of the solution is enforced strongly by eliminating the unknowns of the boundary of cell (0,0) with cells (1,0), (0,1) and (1,1) using the PBC (1). Therefore, contributions to a matrix entry involving the image $\mathbf{J}(q^{n,m})$ of unknown $\mathbf{J}(q)$ in the (n,m) cell should be replaced as follows

$$A(p,q) = A(p,q^{n,m}) \exp\{-jn\mathbf{k}^i \cdot \mathbf{T}_1 - jm\mathbf{k}^i \cdot \mathbf{T}_2\}. \quad (13)$$

We want to use a PMCHWT formulation in all the homogeneous regions for consistency and accuracy and for an easier treatment of junction cases. The PMCHWT formulation consists in summing the contribution of the integral operators on both sides of a surface. The question for the pseudoperiodic PMCHWT formulation with fictitious surfaces is how to get the contributions coming from the neighboring cells.

For a test function $\psi_J(q)$ between the (0,0) and $(-1,0)$ cells, the PMCHWT involves terms from the entire boundary of the $\mathbb{R}^1(0,0)$ and $\mathbb{R}^2(-1,0)$ regions.

We remark that the contribution from region $\mathbb{R}^2(-1,0)$ to a test function $\psi_J(q)$ can be obtained from the contribution from region $\mathbb{R}^2(0,0)$ to the corresponding test function $\psi_J(q^{1,0})$ and the PBC (1). Contributions $A(q^{n,m},p)$ to a matrix entry involving the image $\psi_J(q^{n,m})$ of a test function $\psi_J(q)$ in the (n,m) cell can be computed with:

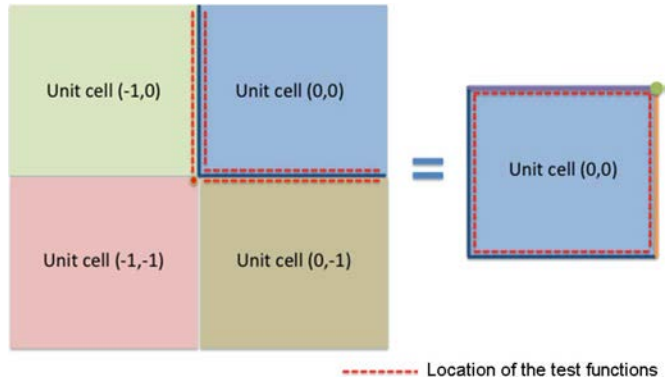

Fig. 5. **Left**: The PMCHWT formulation involves terms from four different unit cells. **Right**: Those terms can be obtained through phase relations with the terms that are directly available in the reference unit cell.

$$A(q,p) = A(q^{n,m},p) \exp\{jn\mathbf{k}^i \cdot \mathbf{T}_1 + jm\mathbf{k}^i \cdot \mathbf{T}_2\}. \quad (14)$$

Some edges belong to four regions of Fig. 4 (e.g. $\mathbb{R}^1(0,0)$, $\mathbb{R}^2(-1,0)$, $\mathbb{R}^1(0,-1)$ and $\mathbb{R}^2(-1,-1)$); on such edges, there are contributions from the entire boundary of these four regions. Each of the last three contributions is obtained from a $\mathbb{R}^1(0,0)$ contribution and (14).

All the contributions will be computed from those of the (0,0) cell (Fig. 5), by looping over the elements bounding the regions of the reference cell and applying the PBC relations (13) and (14), accordingly to the source and reception elements. This scheme also applies to the top and bottom surface and to complex junctions (e.g. when there are several arbitrary internal PEC or dielectric regions, thin sheets, impedance boundary conditions. . .).

III. Efficient Computation of the Integral Operators on the Top and Bottom Boundaries

A. Structured Mesh on Top and Bottom Boundaries

We use RWG and rooftop elements on composite meshes made of triangles and quadrangles. Only the top and bottom regions contributions will involve computations of the pseudoperiodic Green's function. If the boundaries of the top and bottom regions are planar, it is possible to use a structured mesh made of identical quadrangles. If the top (resp. bottom) boundary is not, we suggest to add a fictitious slab on the top (resp. bottom) of the biperiodic structure, in order to use a structured mesh on its top (resp. bottom) boundary, as illustrated on Fig. 6.

B. Use of the Algorithm for Planar FSS Screens

The algorithm for planar FSS of [1], [3] is based on the PEC or resistive version of the EFIE (2). In fact, this algorithm leads to a highly efficient discretization of the L_d operator with the pseudoperiodic Green's function for a planar surface discretized with identical rooftop elements. This is precisely what we need to compute the contributions of the upper and lower regions to the PMCHWT formulation, since $\hat{n} \times \overline{K}_d(\overrightarrow{M}_S) = 0$ and $\hat{n} \times \overline{K}_d(\overrightarrow{J}_S) = 0$ on the planar surfaces bounding these regions.

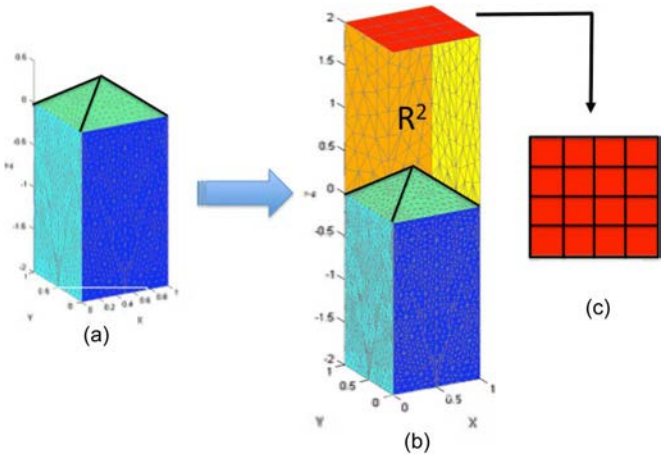

Fig. 6. Adding a fictitious slab $\mathbb{R}^2$ above the biperiodic scattering structures (a) makes it possible to have a structured mesh (c) on the top and bottom surfaces of the entire mesh (b).

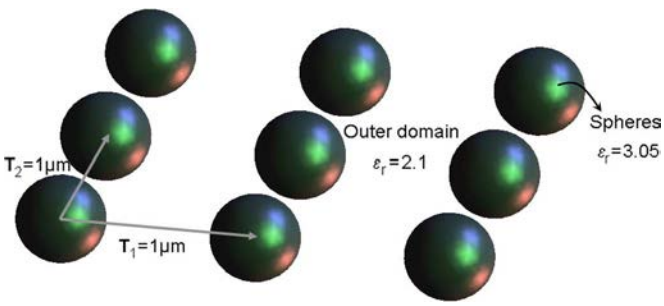

Fig. 7. Array of dielectric spheres in a dielectric outer region. The radii of the spheres is taken to be 0.2 μm or 0.23 μm.

The computation time of the contributions obtained with the planar FSS algorithm is much shorter than what is needed to compute the integral operators in the 3D case. The overall assembly time of this pseudoperiodic SIE method is then similar to that of a 3D SIE with the same number of degrees of freedom.

IV. Validation

The validation of the method has been carried out extensively in [18]. Here three cases are presented, that correspond to two different frequency ranges: infrared (IR) and radar frequencies. For all validation cases, we have used a direct solution method to solve the discretized linear system.

A. Array of Dielectric Spheres at Near IR Wavelengths

1) Description: The first test case consists in a square array of dielectric spheres embedded in a dielectric infinite region. This test case was suggested by T. Teperik [19] and is illustrated on Fig. 7.

The lattice constants are 1 μm. The relative permittivity of the outer region is 2.1 and the relative permittivity of the spheres is 3.05.

We compute the transmission efficiency under normal incidence for wavelengths from 1.448 μm to 1.460 μm in vacuum for two spheres radii $\mathrm{a}_1 = 0.2$ μm and $\mathrm{a}_2 = 0.23$ μm.

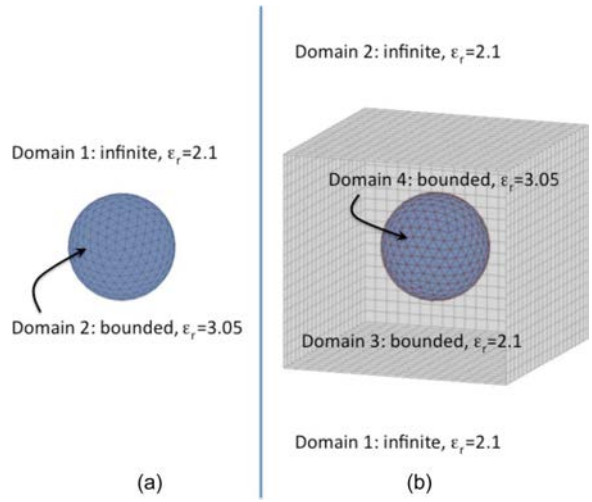

Fig. 8. (a) Mesh of a single free stranding dielectric sphere. (b) Mesh with fictitious surfaces, with structured mesh on top and bottom surfaces.

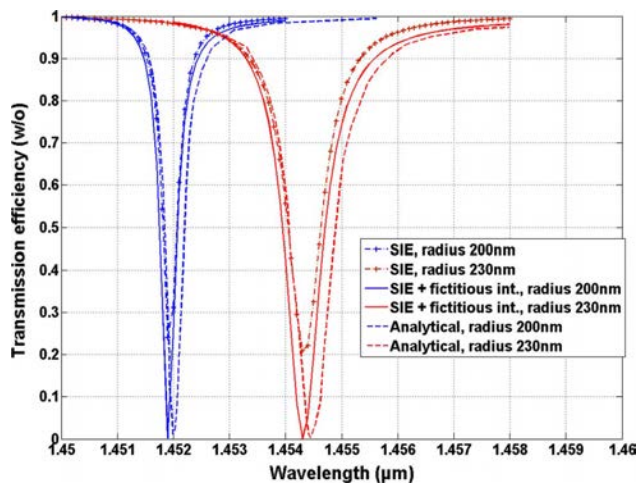

Fig. 9. Comparison between analytical approach and numerical modeling (with and without fictitious surfaces) for two arrays of dielectric spheres (radii 200 nm and 230 nm).

2) Modeling: To assess the effect on accuracy and computation time of fictitious surfaces, the case has been computed with and without fictitious surfaces.

For the first model (cf. Fig. 8(a)), the pseudoperiodic Green's function is used for the external region and the free-space Green's function for the internal region. A single model with 2160 unknowns is used for both radii and corresponding to an average edge length of $\lambda_d/17.9$, where λ_d is the wavelength in the dielectric sphere. Since the number of unknowns is small, we didn't try to use a mesh with a minimal number of unknowns.

In the second model (Fig. 8(b)) we add fictitious surfaces meshed with rectangles with $\lambda_d/20$ edge length. The total number of unknowns is now 7808.

3) Results and Computation Time: We present the transmission efficiency under normal incidence computed with our method and fictitious surfaces, with an asymptotic model [19] and with our method without fictitious surfaces on Fig. 9. There

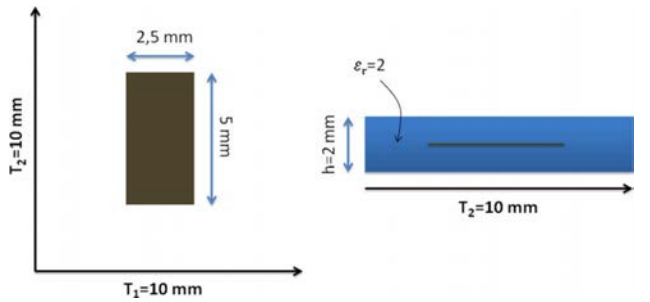

Fig. 10. Scheme of the FSS embedded in a dielectric slab: (a) in the xy-plane (b) in the yz-plane.

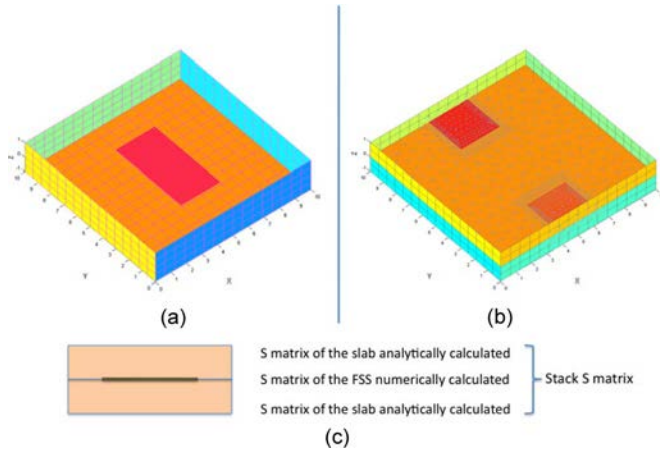

Fig. 11. Three different modeling of a FSS made of an array of perfectly conducting patches embedded in a dielectric slab: (a) BEM modeling where the unit cell consists of a patch embedded in a "box" of dielectric (b) BEM modeling where each patch is placed on two translated unit cells (c) Stack calculation with FSS algorithm.

is very good accuracy between all the results with a slight frequency shift, which is negligible compared to the wavelength.

The computation is carried out with an Intel Itanium II node with 8 processors at 1.4 GHz. Without fictitious surfaces, the computation time is 0.44 h for one wavelength; 99.9% of which is matrix assembly time. With fictitious surfaces, the computation time is only 0.028 h, 82% of which being spent during the matrix assembly. In this case, the fictitious surfaces add a lot of extra degrees of freedom (3.2 times more than without the fictitious surfaces) but even in this case the total computation time is improved by a factor 15.7.

B. FSS at Radar Frequencies

1) Description: We consider now the case of a square array of perfectly conducting rectangular patches embedded in a dielectric slab.

The patches are 5 mm long and 2.5 mm wide with lattice constants of 10 mm along the x and y directions. The FSS is placed in the median plane of a 2 mm thick dielectric slab with $\varepsilon_r = 2$ and $\mu_r = 1$. The geometrical and material characteristics of this case are illustrated on Fig. 10.

2) Modeling: In a first model (Fig. 11(a)), the patch is in the middle of the symmetry cell. There are 3464 unknowns and the maximal edge length at 24 GHz is $\lambda_d/14.2$, where λ_d is the wavelength in the dielectric region.

With the second model, we test junctions through fictitious surfaces. We set the patch across the fictitious side walls (Fig. 11(b)) also adding a horizontal fictitious surface. The surface of the PEC patch is considered as two separate surfaces with one set of ψ_J test functions on each side of the patch. On junction edges between the patch and the horizontal fictitious surface, there is only one ψ_J test function. There are 7050 unknowns. The maximal edge length at 24 GHz is $\lambda_d/9.6$. On this simple geometry, reference results are obtained with a planar FSS code based on [1], as shown on Fig. 11(c).

3) Results: We compare the reflection efficiencies for TE (H) and TM (V) polarizations, at normal and 30° incidences on Figs. 12 and Fig. 13. The comparison between the three models is very good, indicating that there are no significant errors due to fictitious surfaces and to junctions with the fictitious surfaces.

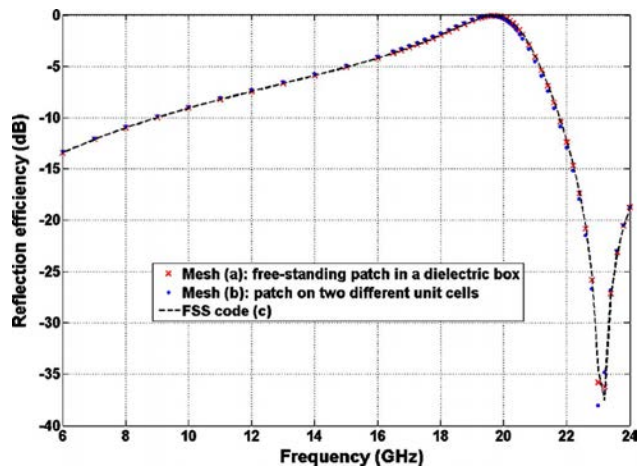

Fig. 12. Reflection efficiency of the array of metallic patches embedded in a dielectric layer under normal incidence.

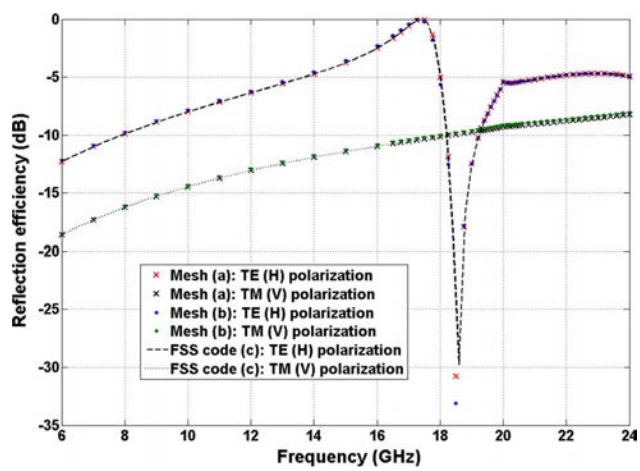

Fig. 13. Reflection efficiency of the array of metallic patches embedded in a dielectric layer under oblique incidence (30°) for TE and TM polarizations.

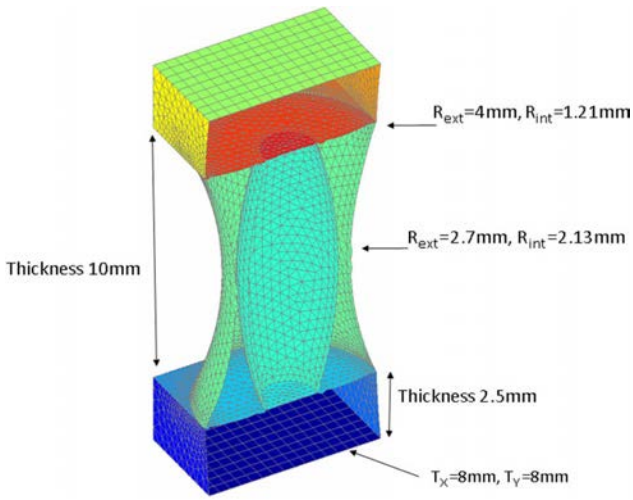

Fig. 14. Geometrical parameters and mesh of the unit cell of the array of evolutive coaxial cavities in a perfectly conducting slab.

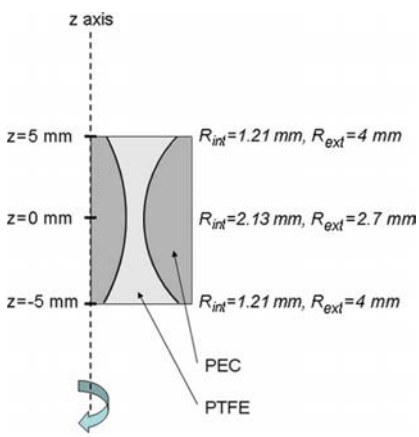

Fig. 15. The cavity is created by rotating two arcs of circle around the z axis. The circles are passing by three points given by the inner and outer radii in $z = 0$ mm and $z = \pm 5$ mm.

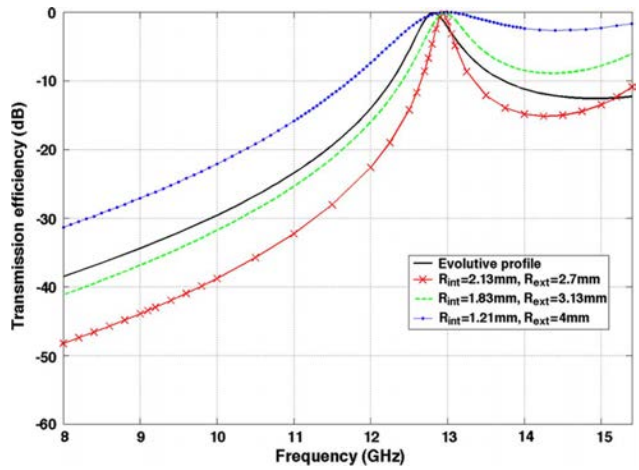

Fig. 16. Transmission efficiency of the array of evolutive coaxial cavities under oblique incidence (64°) and TE (H) polarization: comparison with arrays of straight coaxial cavities.

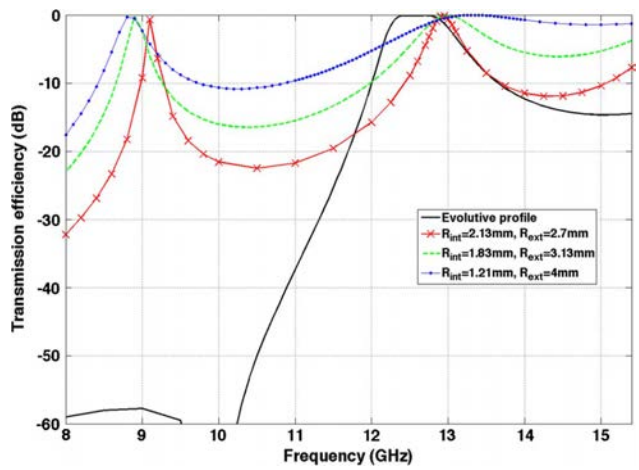

Fig. 17. Transmission efficiency of the array of evolutive coaxial cavities under oblique incidence (64°) and TM (V) polarization: comparison with arrays of straight coaxial cavities.

C. Array of Evolutive Coaxial Cavities in a Perfectly Conducting Metallic Slab

An array of straight coaxial cavities in a silver slab in the visible optical wavelengths has been presented in [20]. This structure has band-pass properties, which are independent on the polarization and on the angle of incidence. It was shown that these properties are due to a resonance of the TE11 mode of the waveguides. Total transmission is not achieved though, due to losses in the silver slab.

We present here a structure based on evolutive coaxial cavities in X band which is a broadband filter under oblique incidence in the TM polarization.

1) Description: The coaxial cavities are arranged in a square lattice 8 mm × 8 mm. The perfectly conducting slab is 10 mm thick. The cavities have a horn-like shape whose vertical section is defined on Fig. 14 and Fig. 15. The cavities are filled with PTFE, with a refractive index of $n_{PTFE} = 1.58$ in order to reduce the frequency for the first TE11 resonance.

2) Modeling: Two fictitious slabs of air are added in order to use locally structured meshes on the top and bottom boundaries. There are 16488 triangles and 512 quadrangles on the mesh we used and 31552 unknowns. All the edges are shorter than $\lambda_d/21$ at the highest frequency, even in the PTFE. The mesh is shown on Fig. 14.

3) Results and Computation Time: The computation is carried out with an Intel Itanium II node with 8 processors at 1.4 GHz. Both the matrix assembly and the direct resolution are parallelized. For one frequency and one incidence, the computation time is 1.3 h.

The transmission efficiencies under oblique incidence at 30° in both TE (H) and TM (V) polarizations are presented on Fig. 16 and Fig. 17 and compared to arrays of straight cavities (narrow, wide or median). The bandwidth is narrow in TE polarization. But the bandwidth in TM polarization is larger with a flat-top of 0.6 GHz. This phenomenon is due to a coupling between the TE11 and TEM coaxial modes in TM polarization (cf. [21], [22]).

V. Conclusion

We have introduced a general method to model the scattering by complex doubly periodic structures, which is based on a single PMCHWT formulation for all regions.

The inner regions are bounded by using fictitious surfaces between translated unit cells. In these regions, the free-space Green's function is used with PBC. We have shown how to derive the PMCHWT contributions from regions neighboring the symmetry cell from terms internal to the symmetry cell. This integral formulation ensures the best accuracy of the final results. The assembly time of the part of the matrix corresponding to the inner region is similar to what we would have had with a 3D case.

The pseudoperiodic Green's function must be used on the top and bottom boundaries. These contributions can be efficiently computed by using an adaptation of the algorithm for planar FSS. The assembly time for these contributions is negligible, due to the local Toeplitz matrix.

Examples of calculation and computation times have been given. They highlight the reduction of the computation time due to the use of fictitious surfaces: for the array of dielectric spheres, it was reduced by a factor 15.7.

The method is a general formulation for arbitrary geometries combining PEC and dielectric regions and all possible junctions used in 3D models. Localized or surface impedance conditions and thin wires can be taken into account. Furthermore, the method can be extended to include a local coupling with the finite element method to handle anisotropic materials.

References

[1] R. Mittra, C. H. Chan, and T. Cwik, "Techniques for analysing frequency selective surfaces—A review," *Proc. IEEE*, vol. 76, no. 12, pp. 1593–1615, Dec. 1988.

[2] T. A. Cwik and R. Mittra, "Scattering from a periodic array of free-standing arbitrarily shaped perfectly conducting or resistive patches," *IEEE Trans. Antennas Propag.*, vol. 35, pp. 1226–1234, Nov. 1987.

[3] C. H. Chan and R. Mittra, "On the analysis of frequency-selective surfaces using subdomain basis functions," *IEEE Trans. Antennas Propag.*, vol. 38, pp. 40–50, Jan. 1990.

[4] R. A. Kipp and C. H. Chan, "A numerically efficient technique for the method of moments solution for planar periodic structures in layered media," *IEEE Trans. Microwave Theory Tech.*, vol. 42, pp. 635–643, Apr. 1994.

[5] P. Harms, R. Mittra, and W. Ko, "Implementation of the periodic boundary-condition in the finite-difference time-domain algorithm for FSS structures," *IEEE Trans. Antennas Propag.*, vol. 42, pp. 1317–1324, Sept. 1994.

[6] J. M. Jin, *The Finite Element Method in Electromagnetics*. New York: Wiley, 1993.

[7] J. M. Jin, *Finite Element Analysis of Antennas and Arrays*. New York: Wiley, 2009, ch. 9.

[8] G. Valerio, P. Baccarelli, P. Burghignoli, and A. Galli, "Comparative analysis of acceleration techniques for 2-D and 3-D Green's functions in periodic structures along one and two directions," *IEEE Trans. Antennas Propag.*, vol. 55, pp. 1630–1643, June 2007.

[9] X. Dardenne and C. Craeye, "Method of moments simulation of infinitely periodic structures combining metal with connected dielectric objects," *IEEE Trans. Antennas Propag.*, vol. 56, pp. 2373–2380, Aug. 2008.

[10] D. T. McGrath and V. P. Pyati, "Phased array antenna analysis with the hybrid finite element method," *IEEE Trans. Antennas Propag.*, vol. 42, pp. 1625–1630, Dec. 1994.

[11] L. C. Trintinalia and H. Ling, "Integral equation modeling of multilayered doubly-periodic lossy structures using periodic boundary condition and a connection scheme," *IEEE Trans. Antennas Propag.*, vol. 52, no. 9, pp. 2253–2261, Sep. 2004.

[12] A. J. Poggio and E. K. Miller, "Integral equation solutions of three-dimensional scattering problems," in *Computer Techniques for Electromagnetics*, R. Mittra, Ed., 2nd ed. New York: Pergamon Press, 1973, pp. 159–264.

[13] L. N. Medgyesi-Mitschang, J. M. Putnam, and M. B. Gedera, "Generalized method of moments for three-dimensional penetrable scatterers," *J. Opt. Soc. Am. A*, vol. 11, no. 4, pp. 1383–1398, Apr. 1994.

[14] J.-M. Jin, "A highly robust and versatile finite element-boundary integral hybrid code for scattering by BOR objects," *IEEE Trans. Antennas Propag.*, vol. 53, pp. 2274–2281, Jul. 2005.

[15] W. C. Chew, J.-M. Jin, E. Michielssen, and J. Song, *Fast and Efficient Algorithms in Computational Electromagnetics*. Norwood, MA: Artech House, 2001.

[16] J.-J. Angélini, C. Soize, and P. Soudais, "Hybrid numerical method for harmonic 3-D Maxwell equations: Scattering by a mixed conducting and in homogeneous anisotropic dielectric medium," *IEEE Trans. Antennas Propag.*, vol. 41, Jan. 1993.

[17] B. M. Kolundžija, "Electromagnetic Modeling of Composite Metallic and Dielectric Structures," *IEEE Trans. Microwave Theory Tech.*, vol. 47, pp. 1021–1032, Jul. 1999.

[18] S. Nosal, "Modélisation électromagnétique de structures périodiques et matériaux artificiels" (in French) Ph.D. dissertation, Ecole Centrale Paris, Châtenay-Malabry, France, 2009 [Online]. Available: http://theses.abes.fr/2009ECAP0030

[19] T. Teperik, R. Sainidou, and F. J. Garcia de Abajo, "Electromagnetic mode trapping for giant optical field enhancement," presented at the META'08, NATO Advanced Research workshop on Metamaterials for Secure Information and Communication Technologies Marrakesh, Morocco, 2008.

[20] D. Van Labeke, D. Gérard, B. Guizal, F. I. Baida, and L. Li, "An angle-independent Frequency Selective Surface in the optical range," *Optics Expr.*, vol. 14, no. 25, 2006.

[21] F. I. Baida, "Enhanced transmission through subwavelength metallic coaxial apertures by excitation of the TEM mode," *Appl. Phys. B*, vol. 78, 2008.

[22] S. Nosal, P. Soudais, and J.-J. Greffet, "Enhancing the bandwidth of coaxial aperture arrays in the radar frequencies," presented at the META'10, 2nd Int. Conf. on Metamaterials, Photonic Crystals and Plasmonics, Cairo, Egypt, 2010.